Journal of Materials Chemistry C

Facile synthesis of multi-resonance ultra-pure-green TADF emitters based on bridged diarylamine derivatives for efficient OLEDs with narrow emission

Journal:	*Journal of Materials Chemistry C*
Manuscript ID	TC-ART-03-2021-001427.R1
Article Type:	Paper
Date Submitted by the Author:	13-May-2021
Complete List of Authors:	Liu, Guanting; Yamagata univ., Organic Materials Science Sasabe, Hisahiro; Yamagata univ., Organic Materials Science Kumada, Kengo; Yamagata univ., Organic Materials Science Matsunaga, Amane ; Yamagata univ., Organic Device Engineering Katagiri, Hiroshi; Yamagata University, Graduate School of Science and Engineering Kido, Junji; Yamagata univ., Organic Materials Science

Facile synthesis of multi-resonance ultra-pure-green TADF emitters based on bridged diarylamine derivatives for efficient OLEDs with narrow emission

Guanting Liu[1], Hisahiro Sasabe[1,2,3], Kengo Kumada[1], Amane Matsunaga[1], Hiroshi Katagiri[1,2,3] and Junji Kido[1,2,3]**

[1]Department of Organic Materials Science, Graduate School of Organic Materials Science, Yamagata University, 4-3-16 Jonan, Yonezawa, Yamagata 992-8510, Japan, [2]Research Center for Organic Electronics (ROEL), Yamagata University, 4-3-16 Jonan, Yonezawa, Yamagata 992-8510, Japan, [3]Frontier Center for Organic Materials (FROM), Yamagata University, 4-3-16 Jonan, Yonezawa, Yamagata 992-8510 (Japan)

E-mail: (h-sasabe@yz.yamagata-u.ac.jp, kid@yz.yamagata-u.ac.jp)

Abstract

High color-purity emission with a minimum full width at half maximum (FWHM) is critical for high-resolution displays. Despite the increasing demand for narrow-band emission materials with multi-resonance-induced thermally activated delayed fluorescence (MR-TADF), their development remains challenging from the viewpoint of synthetic chemistry. In this study, we developed a novel one-pot borylation method that does not require the use of hazardous *tert*-BuLi, and for which the starting materials are not limited to aromatic fluorides and carbazole-based materials. We achieved this by making simple modifications to a boron-nitrogen skeleton. By inserting carbon and oxygen into the skeleton, we created two types of highly efficient green-emitting MR-TADF emitters, namely **DMAc-BN** and **PXZ-BN**. This design enabled the suppression of aggregation-induced quenching, which was one of the major challenges faced by MR-TADF emitters developed in the past. OLEDs using our **DMAc-BN** and **PXZ-BN** emitters

exhibited external quantum efficiencies of 20.3% and 23.3%, respectively, with FWHM values of 49 and 47 nm, respectively. **PXZ-BN** exhibited pure green emission with CIE coordinates of (0.22, 0.67).

Keywords: Thermally activated delayed fluorescence • Organoboron compound • Borylation • Organic light-emitting device

Introduction:

Highly efficient thermally activated delayed fluorescence (TADF) was first reported by Adachi et al.[1], and was a major breakthrough for OLEDs, because it paved the way for achieving 100% internal quantum efficiency without the need for precious metal component [2-8]. The small singlet-triplet (S_1-T_1) energy gaps (ΔE_{ST}) of TADF materials enable efficient reverse intersystem crossing (RISC) from T_1 to S_1 and the use of all generated excitons. To minimize ΔE_{ST}, conventional TADF materials require electron-rich donors (D) and electron-deficient acceptor (A) fragments that reduce the overlap between the lowest unoccupied molecular orbitals (LUMOs) and the highest occupied molecular orbitals (HOMOs). This strategy has been validated numerous times and can be used to achieve efficient TADF characteristics. A variety of high-performance OLEDs designed using this concept have been manufactured, with external quantum efficiencies (EQEs) of over 30%[9-14]. However, when this strategy is used, structural relaxation occurs in the excited state, and OLEDs exhibit large Stokes shifts and broad emission spectra, which directly impact color purity and device performance.

Instead of conventional D-A conjugated emitters, Hatakeyama et al. reported TADF emitters (**DABNA-1 Scheme 1**) that used a new type of multi-resonance thermally activated delayed fluorescence (MR-TADF) [15-17]. In the compound, due to the complementary resonance effect of

the para-position boron and nitrogen atoms, the electron density between HOMO and LUMO is significantly separated. Because of the rigid molecular framework, a small stroke shift and narrow emission peak were observed, with an FWHM of only 28 nm. However, despite the high EQE (EQE_{max} = 20.2%) and high color purity of MR-TADF emitters, their synthesis requires lithiation by *tert*-BuLi to introduce a boron atom in the first step, making this synthesis extremely hazardous.

In this paper, we report a relatively secure synthesis of the MR effects induced by B-N-containing core-structure molecules (**DMAc-BN** and **PXZ-BN**). We used a one-pot borylation method to simplify the synthesis of **DMAc-BN** and **PXZ-BN**. Initial lithiation is still required for borylation, but *tert*-BuLi is not used. Additionally, the starting materials are not limited to aromatic fluorides (Ar-F) and carbazole-based materials [18-20], which is a critical advantage that would expand the material science and industrial applications of MR-TADF (**Scheme 1**). **DMAc-BN** and **PXZ-BN** show pure green emission, with small FWHMs (33 nm and 38 nm, respectively) and high photoluminescence quantum yields (PLQYs) (88% and 90%, respectively). In addition, the OLED devices that used the emitters had high EQEs: 20.3% for **DMAc-BN** and 23.3% for **PXZ-BN**.

Results and Discussion:

The molecular design is illustrated in **Scheme 1**. Unlike previously reported **DABNA-1**, **DMAc-BN** and **PXZ-BN**[21-23] are inserted either an sp^3 hybridized carbon or oxygen atom; this inserted atom bridges the molecular skeleton. In contrast, the extension of the frontier molecular orbital to the added phenyl units significantly affects the corresponding photophysical properties. In addition, the presence of non-conjugated sp^3 bonds induces helical molecular structure, and expects to reduce the aggregation-induced quenching, which can ultimately lead to higher EQEs.

The compounds **DMAc-BN** and **PXZ-BN** were synthesized in two steps. Under the conditions of Pd(0) as the catalyst and sodium *tert*-butoxide as the base, 9,9-dimethyl-9,10-dihydroacidine and phenoxazine reacted with the commercially available starting material 1,2,3-tribromobenzene through a Buchwald-Hartwig coupling reaction at 110ºC to produce an intermediate **S1** yield of 30% and **S2** yield of 40% (**Scheme S1**). Through a lithium-bromide exchange reaction with *n*-BuLi to promote the electrophilic capture of boron tribromide, boron atom was introduced into the reactor. In addition, intramolecular borylation occurred in the presence of diisopropylethylamine to produce a 38% yield of **DMAc-BN** and 41% yield of **PXZ-BN**. **DMAc-BN** and **PXZ-BN** were characterized by ^{1}H NMR, ^{13}C NMR, and ^{11}B NMR spectroscopy; mass spectrometry; and elemental analysis, and purified by temperature-gradient vacuum sublimation.

The helical structures of **DMAc-BN** and **PXZ-BN** were determined by X-ray crystallography (**Figure 1**). The single bonds of C–B and C–N can be confirmed from the bond length, such as C–B bonds were 1.508-1.538 Å in length and C–N bonds were 1.400-1.432 Å in length. The C–O bonds were 1.378-1.386 Å in length for **PXZ-BN**, and the C–C bonds were 1.515-1.540 Å in length for **DMAc-BN**. Because of the longer C–B bonds than C–N bonds, the dihedral angles of the nitrogen-connected phenyl rings (A–B: 54.72°, A–B': 56.44°) are larger than the dihedral angles of the boron-connected phenyl rings (C–C': 32.57°) for **DMAc-BN**. Similar phenomenon was found for **PXZ-BN**; The dihedral angles of the nitrogen-connected phenyl rings (A–B: 39.75°, A–B': 46.83°) are larger than the dihedral angles of the boron-connected phenyl rings (C–C': 35.83°).

MR-dominated frontier orbital distributions were clearly confirmed for **DMAc-BN** and **PXZ-BN** (**Figure 2**), as computed by density functional theory (DFT) calculations. The HOMOs and LUMOs of **DMAc-BN** and **PXZ-BN** spread over the entire skeleton, thereby extending the π-

skeleton, despite their distorted structures. Because of the MR effects, the HOMOs and LUMOs were localized on different atoms, except for the phenyl ring connected to oxygen on the opposition of boron (for **PXZ-BN**) and the phenyl ring connected to carbon on the opposition of boron (for **DMAc-BN**). This can be attributed to the non-conjugated structure caused by the sp^3-hybridized carbons of the acridan subunits and lone pairs of oxygen. The stronger electron-donating capacity of the oxygen atom lowers the HOMO and LUMO energy levels and simultaneously narrows the HOMO–LUMO energy gap. The computed HOMO and LUMO energy levels for **DMAc-BN** and **PXZ-BN** support this assumption (**Figure 2**).

The photophysical properties of the thin-film forms of **DMAc-BN** and **PXZ-BN** (3 wt% doping in 3,3-di(9H-carbazol-9-yl)-1,1-biphenyl (**mCBP**)[24]) are summarized in **Table 1**. A strong absorption band can be observed at 460 nm for **DMAc-BN** and 475 nm for **PXZ-BN** from corresponding ultraviolet (UV)-visible absorption spectrum (**Figure 3**). Narrow green emission peak at 484 nm for **DMAc-BN** and 502 nm for **PXZ-BN** can be observed from fluorescence spectrum at 300 K (**Figure 3**). The Stokes shift/FWHM values were significantly small: 24/33 nm for **DMAc-BN** and 27/38 nm for **PXZ-BN**, suggesting that vibrionic coupling during the transition from S_1 to S_0 was minimized by the non-bonding HOMO and LUMO [16]. Their TADF properties can be proofed from the transient photoluminescence, which showed distinct short-lived prompt fluorescence and long-lived delayed fluorescent properties. Short prompt fluorescence lifetimes (τ_{PF}) of 6.2 and 8.2 ns were observed for **DMAc-BN** and **PXZ-BN**, respectively. Long delayed fluorescence lifetimes (τ_{DF}) of 32.9 and 90.7 μs were observed for **DMAc-BN** and **PXZ-BN**, respectively (**Table 1**). Also, we measured PLQYs of **DMAc-BN**, **PXZ-BN** and **DABNA-1** doped **mCBP** films in different doping concentration. The suppression of aggregation-induced quenching

can be confirmed by the doping concentration dependent PLQYs (**Figure S6**). The PLQYs of **DABNA-1**-doped films were sharply decreased with increasing of doping concentration, but the PLQYs of **DMAc-BN** and **PXZ-BN**-doped films were gradually decreased compared with that of **DABNA-1**. Note that the PLQYs of **DMAc-BN** and **PXZ-BN**-doped films were observed to be apparently higher than that of **DABNA-1** at the higher concentration of 10 % and 20 % most likely due to the helical molecular structure induced by the bridged arylamine units.

To evaluate the device performance of **DMAc-BN** and **PXZ-BN** as emitters, we measured the films of emitters doped in **mCBP**. With respect to solution states, **DMAc-BN** and **PXZ-BN** showed similar but broadened emission peaks when doped with **mCBP** at 3 wt%. **DMAc-BN**:**mCBP**- and **PXZ-BN**:**mCBP**-doped films produced high PLQY values of 88% for **DMAc-BN** and 90% for **PXZ-BN**. These high PLQY values are beneficial to OLED devices. Thus, we fabricated and estimated OLED devices involving **DMAc-BN** and **PXZ-BN** as MR-TADF emitters, with the following device organization: [ITO/triphenylamine-containing polymer: 4-isopropyl-4'-methyldiphenyl-iodonium tetrakis(pentafluorophenyl)borate (**PPBI**) (20 nm) / di-[4-(N,N-ditolyl-amino)-phenyl] cyclohexane (**TAPC**) (15 nm) / **mCBP** (5 nm) / 3 wt% guest-doped **mCBP** (20 nm) / (9-phenyl-9*H*- carbazole-3,6-diyl)bis(diphenylphosphine oxide) (**PO9**) [25] (10 nm) / 3,3''',5,5'-tetra(3-pyridyl)-1,1';3',1'''- terphenyl (**B3PyPB**) [26] (40 nm) / LiF (0.5 nm) /Al (100 nm)]. **mCBP** was inserted between **TAPC** and emission layer to avoid the formation of the electromer of **TAPC**[27] at high current density. Energy diagrams for OLEDs constructed with either **DMAc-BN** or **PXZ-BN** emitters are illustrated in **Figure S1**. The devices using **DMAc-BN** and **PXZ-BN** emitters exhibited green emission at 503 and 516 nm, with FWHMs of 49 and 47 nm and CIE coordinates of (0.18, 0.60) and (0.22, 0.67), respectively (**Figure 4**). Notably, the two devices had high maximum EQEs of 20.3% and 23.3%, respectively; the **PXZ-BN** device had a

slightly higher EQE because its PLQY (90%) was higher than that of the **DMAc-BN** device (88%). Although both **DMAc-BN** and **PXZ-BN** have long τ_{DF}s of 30–90 μs, however, these emitters showed much smaller efficiency roll-off than that of **DABNA-1** (τ_{DF} = 93.7 μs)[15]. It is well-known that the final EQE is determined by the four factors: (i) PLQY, (ii) exciton formation ratio, (iii) outcoupling factor, and (iv) carrier balance. Here, the former three factors, (i)–(iii) are almost similar among **DMAc-BN**, **PXZ-BN**, and **DABNA-1**. Therefore, it can be considered that the suppressed efficiency roll-off was caused by improved carrier balance in different devices. In order to validate this hypothesis, we fabricated three types of devices, Device A–C with **DMAc-BN** emitter, where we tried to investigate the effects of **mCBP** and **PO9** layers toward the carrier balance factor (**Figure S7-S9**). Introduction of **mCBP** in Device B and **PO9** in Device C apparently reduced the current density compared with that in Device A without using these two layers (**Figure S9**). In addition, the much reduced current density was observed when **PO9** was used compared with that of **mCBP**. While, the introduction of **PO9** significantly contributed to increase the maximum EQE up to 5% (Device A vs C in **Figure S8**). Therefore, it can be concluded that **PO9** reduced the electron carriers to improve the carrier balance factor contributing to the higher EQEs. Among newly developed two emitters, **DMAc-BN** exhibited smaller efficicency roll-off compared with the device using **PXZ-BN** because **DMAc-BN** has a shorter τ_{DF} (32.9 μs) compared to that of **PXZ-BN** (τ_{DF} = 90.7 μs).

Conclusion:

In summary, we developed a simplified process for synthesizing novel carbon- and oxygen-bridged MR-TADF emitters (**DMAc-BN**, **PXZ-BN**) using non-hazardous *n*-BuLi. Our newly developed MR-TADF emitters exhibit narrow emission peaks at 50 nm and high quantum yields.

Also, aggregation-induced quenching can be suppressed by a helical molecular structure. In particular, the oxygen-bridged MR-TADF emitter **PXZ-BN** exhibits ultra-pure green emission with CIE coordinates of (0.22, 0.67) and an EQE of 23.3%. The emission colors of MR-TADF emitters can be simply tuned using carbon- or oxygen-bridged structures. Our method can aid the development of OLED displays having superior performance and an expanded color range.

Supporting Information

Supporting information is available.

Acknowledgements:

We gratefully acknowledge the partial financial support from the Center of Innovation (COI) Program of the Japan Science and Technology Agency, JST. H.S. acknowledges partial financial support from JSPS KAKENHI (17H03131, 20H02807).

References:

1 H. Uoyama, K. Goushi, K. Shizu, H. Nomura and C. Adachi, *Nature*, 2012, **492**, 234–238.

2 Z. Yang, Z. Mao, Z. Xie, Y. Zhang, S. Liu, J. Zhao, J. Xu, Z. Chi and M. P. Aldred, *Chem. Soc. Rev.*, 2017, **46**, 915–1016.

3 N. Aizawa, I. N. S. PARK and T. YASUDA, *AAPPS Bull.*, 2016, **26,** 9-19.

4 H. Nakanotani, Y. Tsuchiya and C. Adachi, *Chem. Lett.* DOI:10.1246/cl.200915

5 X. Liang, Z.-L. Tu and Y.-X. Zheng, *Chem. – A Eur. J.*, 2019, **25**, 5623–5642.

6 H. Kaji, H. Suzuki, T. Fukushima, K. Shizu, K. Suzuki, S. Kubo, T. Komino, H. Oiwa, F. Suzuki, A. Wakamiya, Y. Murata and C. Adachi, *Nat. Commun.*, 2015, **6**, 1–8.

7 Y. Liu, C. Li, Z. Ren, S. Yan and M. R. Bryce, *Nat. Rev. Mater.*, 2018. **3**.18020.

8 Y. Im, M. Kim, Y. J. Cho, J.-A. Seo, K. S. Yook and J. Y. Lee, *Chem. Mater.*, 2017, **29**, 1946–1963.

9 T.-A. Lin, T. Chatterjee, W.-L. Tsai, W.-K. Lee, M.-J. Wu, M. Jiao, K.-C. Pan, C.-L. Yi, C.-L. Chung, K.-T. Wong and C.-C. Wu, *Adv. Mater.*, 2016, **28**, 6976–6983.

10 C.-K. Moon, K. Suzuki, K. Shizu, C. Adachi, H. Kaji and J.-J. Kim, *Adv. Mater.*, 2017, **29**, 1606448.

11 D. H. Ahn, S. W. Kim, H. Lee, I. J. Ko, D. Karthik, J. Y. Lee and J. H. Kwon, *Nat. Photonics*, **13,** 540-546.

12 W. Li, M. Li, W. Li, Z. Xu, L. Gan, K. Liu, N. Zheng, C. Ning, D. Chen, Y. Wu and S. Su, *ACS Appl. Mater.,* 2021, **13,** 5302-5311.

13 P. Rajamalli, N. Senthilkumar, P.-Y. Huang, C.-C. Ren-Wu, H.-W. Lin and C.-H. Cheng, *J. Am. Chem. Soc.*, 2017, **139**, 10948–10951.

14 T. Wu, M. Huang, C. Lin, P. Huang, T. Chou, H. Lin, R. Liu and C. Cheng, *Nat. Photonics*, 2018, **12,** 235-240.

15 T. Hatakeyama, K. Shiren, K. Nakajima, S. Nomura, S. Nakatsuka, K. Kinoshita, J. Ni, Y. Ono and T. Ikuta, *Adv. Mater.*, 2016, **28**, 2777–2781.

16 Y. Kondo, K. Yoshiura, S. Kitera, H. Nishi, S. Oda, H. Gotoh, Y. Sasada, M. Yanai and T. Hatakeyama, *Nat. Photonics*, 2019, **13**, 678–682.

17 S. Madayanad Suresh, D. Hall, D. Beljonne, Y. Olivier and E. Zysman-Colman, *Adv. Funct. Mater.*, 2020, **30**, 1908677.

18 Y. Zhang, D. Zhang, J. Wei, Z. Liu, Y. Lu and L. Duan, *Angew. Chemie Int. Ed.*, 2019, **58**, 16912–16917.

19 M. Yang, I. S. Park and T. Yasuda, *J. Am. Chem. Soc.*, 2020, **142**, 19468–19472.

20 Y. Xu, C. Li, Z. Li, Q. Wang, X. Cai, J. Wei and Y. Wang, *Angew. Chemie Int. Ed.*, 2020, **59**, 17442–17446.

21 P. Jiang, L. Zhan, X. Cao, X. Lv, S. Gong, C. Zhou, Z. Huang, F. Ni, Y. Zou, C. Yang, (2021): ChemRxiv. Preprint. https://doi.org/10.26434/chemrxiv.13285847.v1

22 H., Tao. Z. Lisi, L. Nengquan, H. Zhongyan, C. Xiaosong, X. Zhengqi, S. Gong, C. Zhou, C. Zhong, C. Yang, (2021): ChemRxiv. Preprint. https://doi.org/10.26434/chemrxiv.14046296.v1

23 During the preparation of this manuscript, the properties of **DMAc-BN** and **PXZ-BN** were independently reported by Jiang, Tao and co-workers (ref 24,25).

24 P. Schrögel, N. Langer, C. Schildknecht, G. Wagenblast, C. Lennartz and P. Strohriegl, *Org. Electron.*, 2011, **12**, 2047–2055.

25 L. S. Sapochak, A. B. Padmaperuma, X. Cai, J. L. Male and P. E. Burrows, *J. Phys. Chem. C*, 2008, **112**, 7989–7996.

26 H. Sasabe, E. Gonmori, T. Chiba, Y.-J. Li, D. Tanaka, S.-J. Su, T. Takeda, Y.-J. Pu, K. Nakayama and J. Kido, *Chem. Mater.*, 2008, **20**, 5951–5953.

27 J. Kalinowski, G. Giro, M. Cocchi, V. Fattori and P. D. Marco, *App. Phys. Lett.* 2000, **76,** 2352-2354.

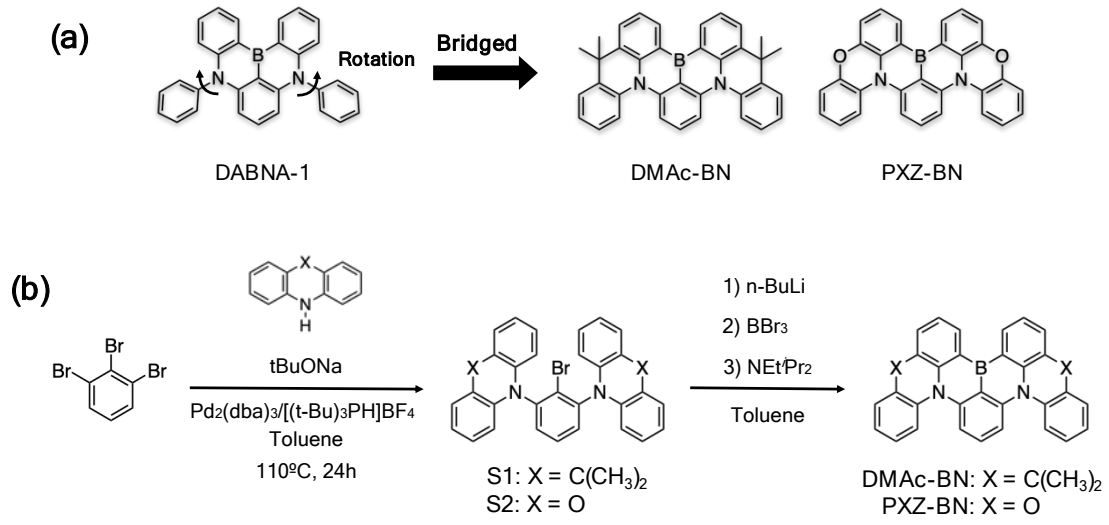

Scheme 1. (a) Molecular design strategy and chemical structures of **DMAc-BN** and **PXZ-BN**; (b) Synthesis of **DMAc-BN** and **PXZ-BN**.

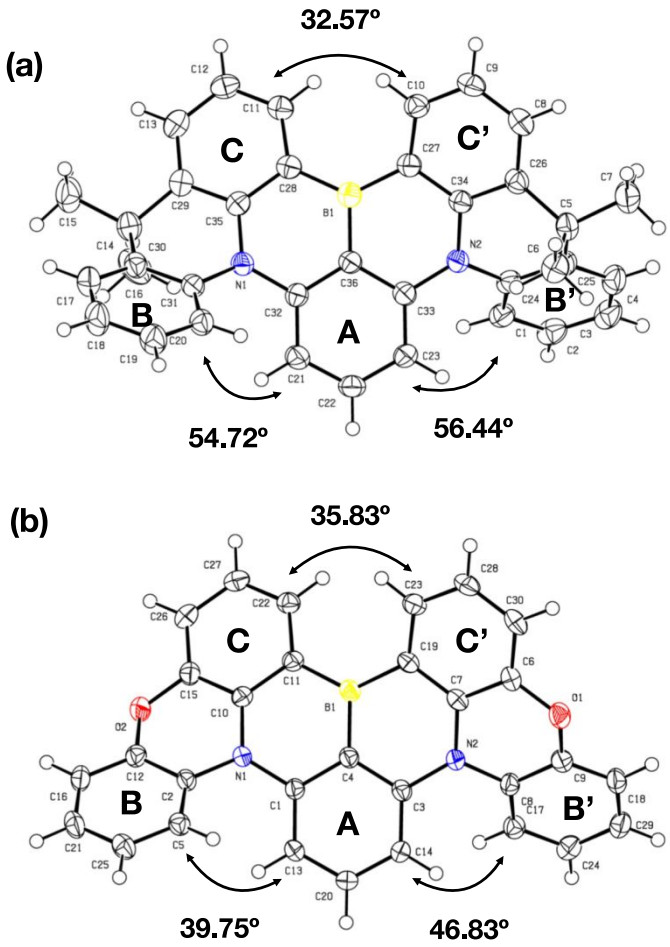

Selected Bond Length

B1–C28	1.533 Å	B1-C27	1.536 Å
B1–C36	1.509 Å		
N1–C35	1.416 Å	N2–C34	1.409 Å
N1–C32	1.409 Å	N2–C33	1.400 Å
N1–C31	1.426 Å	N2–C24	1.432 Å
C14–C29	1.521 Å	C5–C7	1.522 Å
C14–C30	1.515 Å	C5–C6	1.539 Å
C5–C26	1.520 Å	C14–C16	1.540 Å
C5–C25	1.520 Å	C14–C15	1.529 Å

Selected Bond Length

B1–C11	1.533 Å	B1–C19	1.538 Å
B1–C4	1.508 Å		
N1–C10	1.404 Å	N2–C7	1.401 Å
N1–C2	1.418 Å	N2–C8	1.420 Å
N1–C1	1.403 Å	N2–C3	1.401 Å
O2–C15	1.386 Å	O1–C6	1.384 Å
O2–C12	1.379 Å	O1–C9	1.378 Å

Figure 1. ORTEP drawing of (a) **DMAc-BN** and (b) **PXZ-BN** obtained by X-ray crystallography.

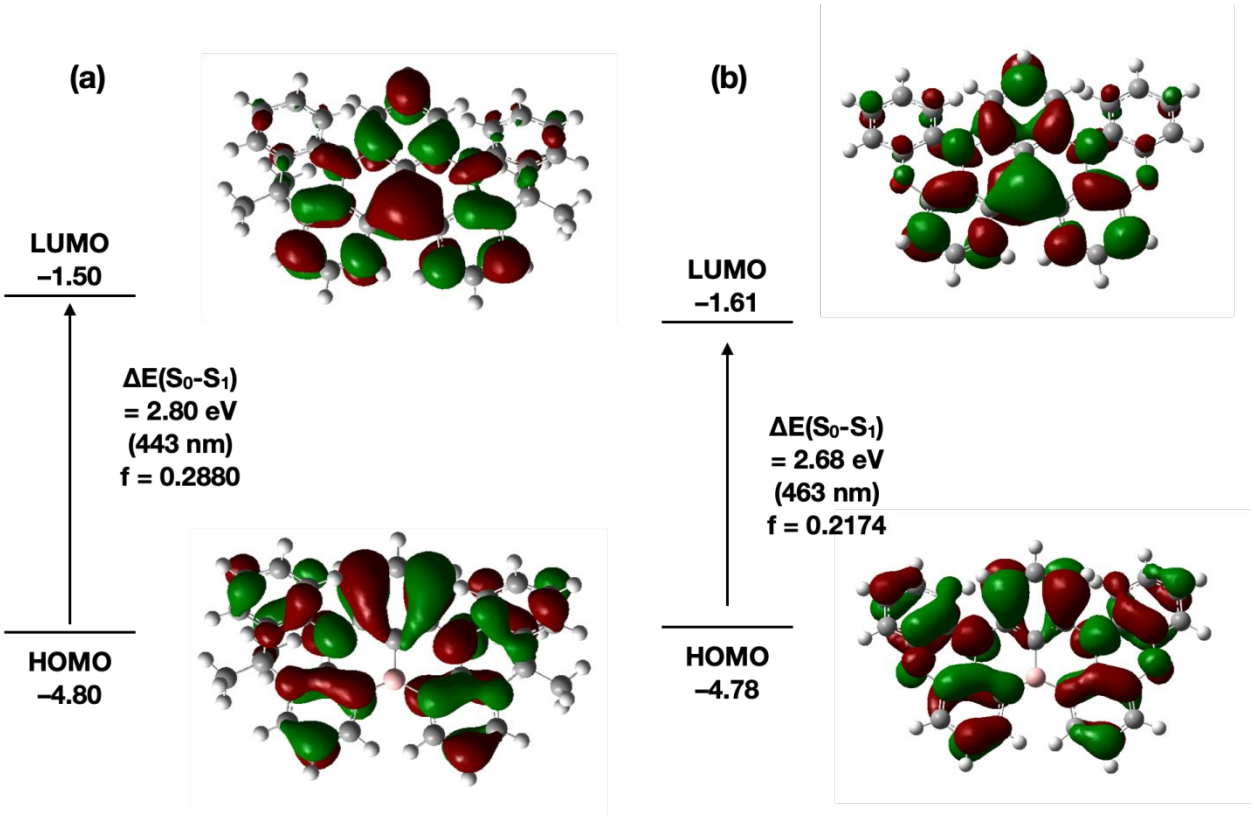

Figure 2. Kohn-Sham molecular orbitals (HOMO and LUMO) and oscillator strength (f) of the S_0-S_1 transition for (a) **DMAc-BN** and (b) **PXZ-BN** calculated at the (TD)B3LYP/6-31G(d).

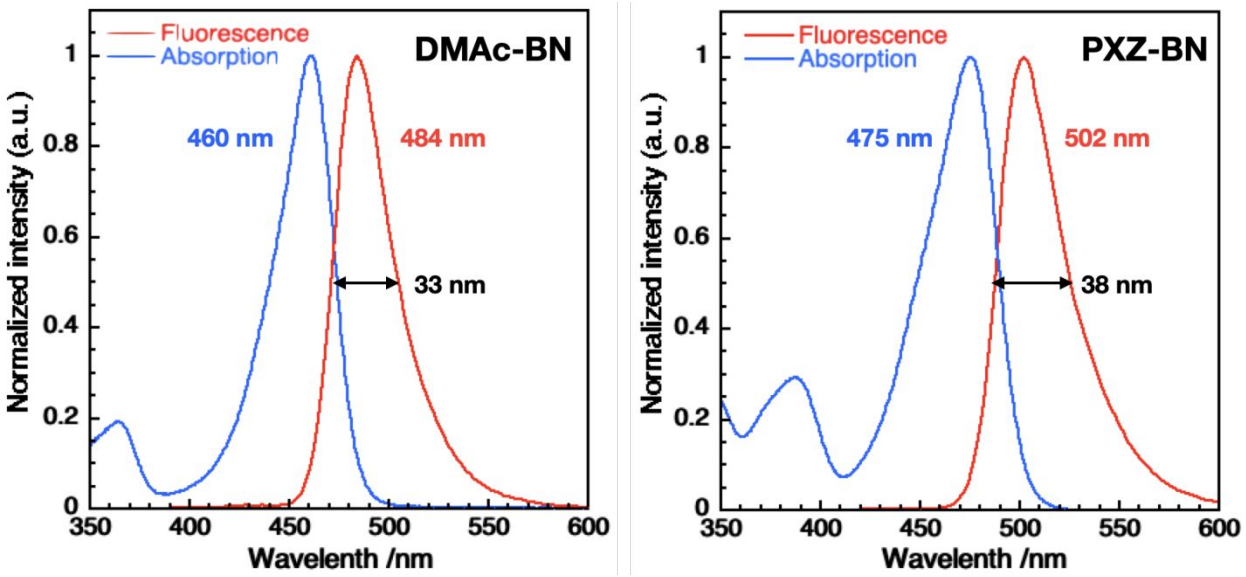

Figure 3. Photophysical properties of **DMAc-BN** and **PXZ-BN**. Absorption and fluorescence spectra (at 300 K) in 2-MeTHF (0.02 mM).

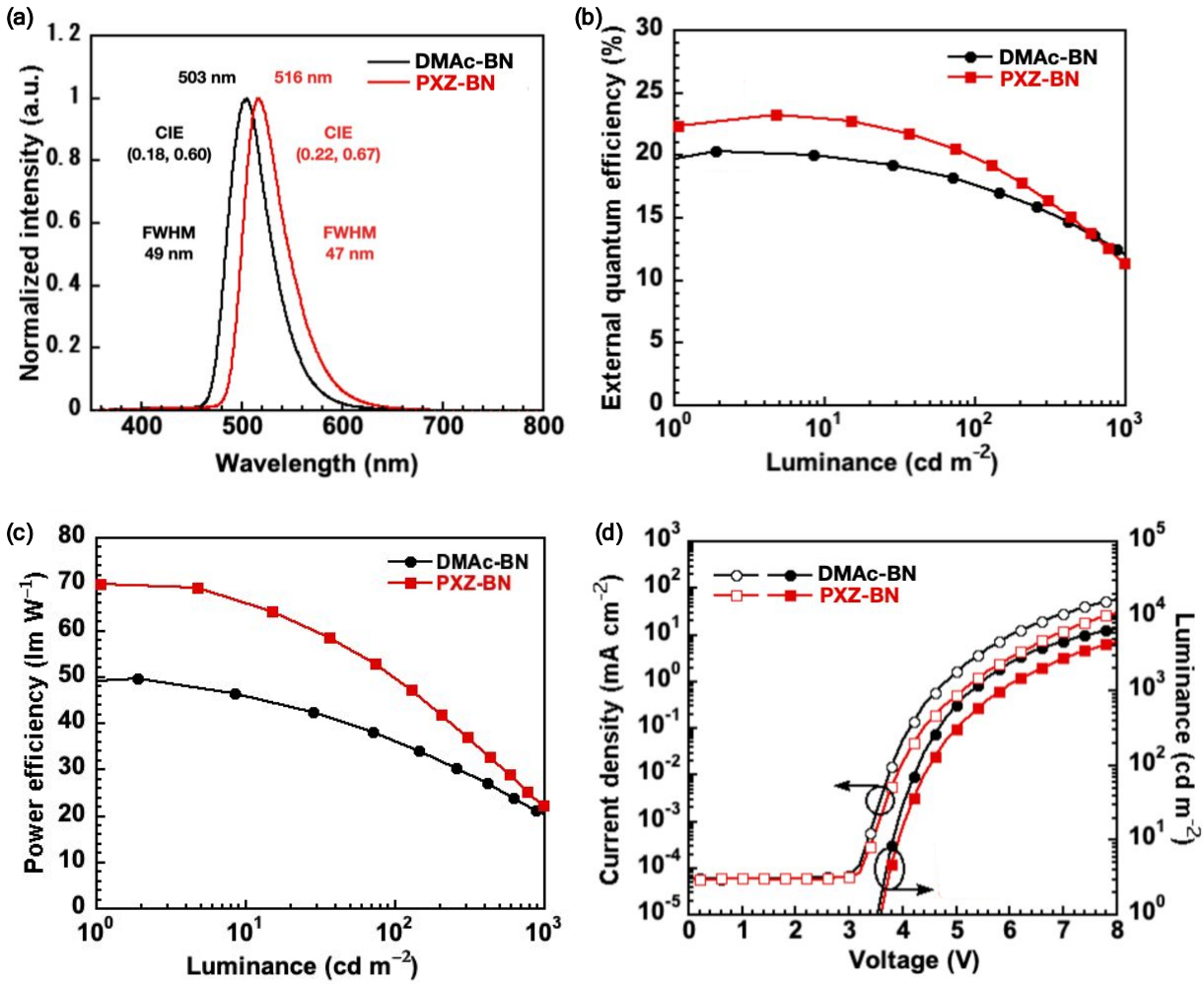

Figure 4. Characteristics of OLEDs fabricated with **DMAc-BN** (black), **PXZ-BN** (red) as emitters. (a) Normalized EL spectra. (b) EQE versus luminance. (c) PE versus luminance. (d) Current density and luminance versus driving voltage.

Table 1. Summary of photophysical properties.

Emitter	λabs^a (nm)	λem^a (nm)	λph^a (nm)	$FWHM^a$ (nm)	$\Delta E_{ST}{}^a$ (eV)	$\Phi_{PL}{}^b$ (%)	$\tau_{PF}{}^b$ (ns)	$\tau_{DF}{}^b$ (μs)	$k_F{}^b$ (10^7 s^{-1})	$k_{IC}{}^b$ (10^6 s^{-1})	$k_{ISC}{}^b$ (10^7 s^{-1})	$k_{RISC}{}^b$ (10^4 s^{-1})
DMAc-BN	460	484	517	33	0.16	88	6.2	32.9	13.1	17.8	1.3	2.4
PXZ-BN	475	502	540	38	0.17	90	8.2	90.7	8.2	9.1	3.1	0.9

[a] Maximum wavelength of UV absorption ($\lambda_{abs,}$ 300 K), fluorescence (λ_{em},300 K), phosphorescence (λ_{ph}, 77 K), FWHM, and S_1-T_1 energy gap (ΔE_{ST}) measured in 0.02 mM 2-MeTHF; [b] absolute PLQY (Φ_{PL}), lifetimes calculated from the fluorescence decay, as well as rate constants for singlet radiative decay (k_F), non-radiative decay (k_{IC}), intersystem crossing (k_{ISC}), and reverse intersystem crossing (k_{RISC}) measured in 3 wt%-doped films of emitters in **mCBP**.